Journal of Power Electronics, Vol. 17, No. 1, pp. 11-19, January 2017

JPE 17-1-2

https://doi.org/10.6113/JPE.2017.17.1.11
ISSN(Print): 1598-2092 / ISSN(Online): 2093-4718

A Hybrid DC/DC Converter for EV OBCs Using Full-bridge and Resonant Converters with a Single Transformer

Najam ul Hassan*, Yoon-Jae Kim*, Byung-Moon Han*, and Jun-Young Lee†

*,†Department of Electrical Engineering, Myongji University, Yongin, Korea

Abstract

This paper proposes a dc/dc converter for electric vehicle onboard chargers using a secondary resonant tank. To attain soft switching characteristics, such as zero voltage switching, magnetizing inductance has been used at the primary side of the transformer. The leakage inductance of the transformer is used as a resonant inductor on the secondary side to avoid the use of a separate inductor as resonance. The proposed converter is applicable for a wide load range. A 6.6KW prototype has been implemented for a wide range of load variations (250V, 330V, 360V, and 413V). A maximum efficiency of 97.4% is achieved at 413V.

Key words: Battery charger, DC/DC converter, Hybrid converter

I. INTRODUCTION

Due to concerns over climate change and air polution in large urban cities, the demand for plug in hybrid electric vehicles (PHEVs) and electric vehicles (EVs) has been increasing over the years [1], [2]. High capacity battery packs have been extinsively used in PHEVs and EVs. These battery packs demand high efficiency, low cost and compact chargers. Among the existing solutions, the most common charger architecture consists of an AC/DC converter with power factor correction and an isolated DC/DC converter [3]-[5]. High efficiency is the main requirement for power converter topologies [6]. An onboard charger (OBC) is mounted on EVs and PHEVs to charge the batteries [7]. Until now, OBCs with a charging capacity of 3.3KW have been used in PHEV/EVs and they take approximately 8 hours to charge the batteries [8], [9]. A solution for minimizing the charging time by doubling the charging capacity of chargers is underway [10].

The DC/DC converter topologies use for OBCs should meet several requirements, such as, (a) wide output voltage control, (b) soft-switching in the primary switches under different load and battery voltages, (c) a low voltage rating in the secondary rectifiers, (d) the reduction of unnecessary loss by avoiding snubber circuits, (e) the switching frequency variation should be narrow to reduce the switching loss and to eliminate audible noise under wide load and battery voltages, and (f) the circulating current should be minimized [11].

In this paper, a hybrid PWM DC/DC converter comprised of a FB converter and a PWM resonant converter for EV OBCs is suggested. The proposed converter has operational characteristics that are a mixture of the resonant converter and the FB converter. Unlike previous hybrid converters, the resonant converter and FB converter use PWM operation so that the transformer structure can be simplified by coupling the two secondary sides. The proposed structure provides additional merits such as no dissipative snubber circuitry and no output filter. The ZV-ZCS operation of the bottom switches and the ZVS operation of the top switches can be accomplished by proper design of the resonant. Since the design of the proposed converter is related to various parameters such as the resonant tank, the transformer turns-ratio, the magnetizing inductance, and the duty-ratio, a design procedure is suggested. Based on this design procedure, the proposed converter is implemented and tested using a 6.6kW charger.

II. PROPOSED CONVERTER

A. Description of the Proposed Converter

Manuscript received Jun. 7, 2016; accepted Nov. 11, 2016
Recommended for publication by Associate Editor Yan Xing.
†Corresponding Author: pdpljy@mju.ac.kr
Tel: +82-330-6357, Fax: +82-330-6977, Myongji University
*Department of Electrical Engineering, Myongji University, Korea

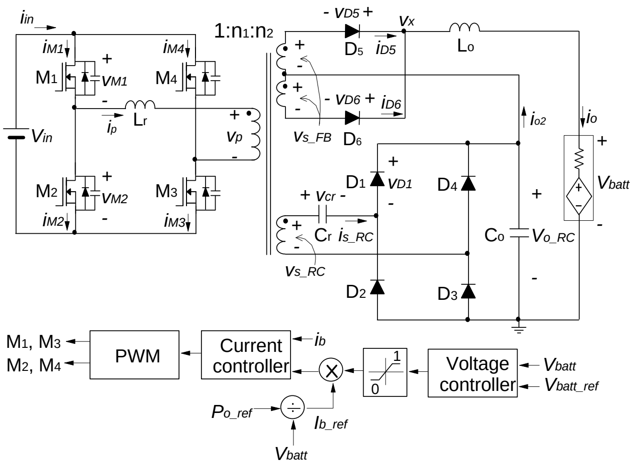

Fig. 1. Schematic diagram of the proposed converter.

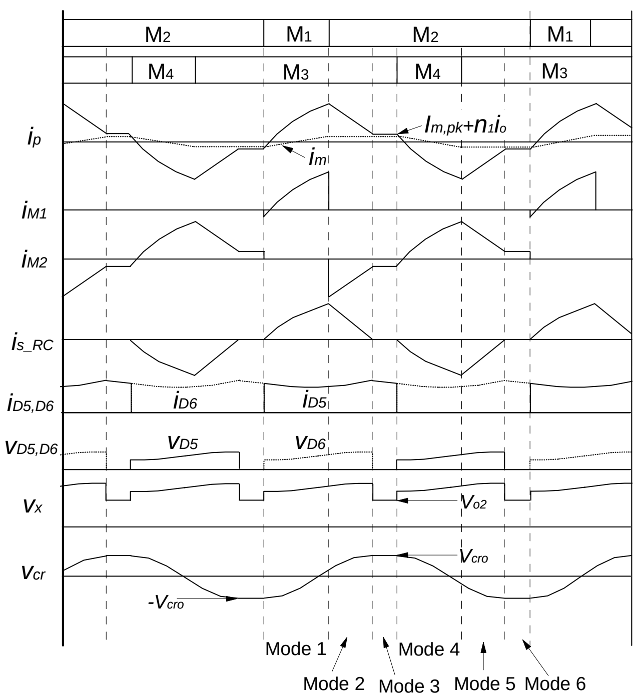

Fig. 2. Key waveforms of the proposed converter.

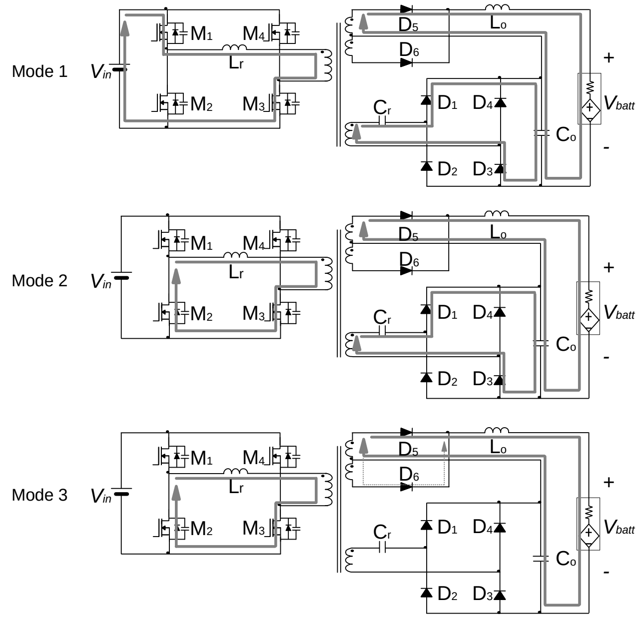

Fig. 3. Operational mode diagrams.

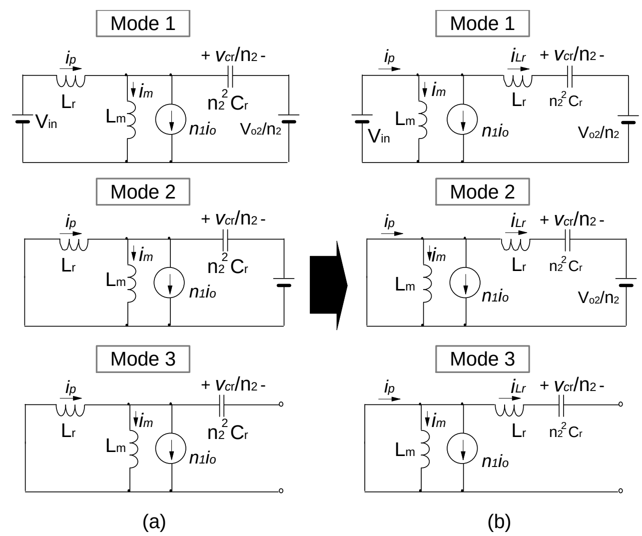

Fig. 4. (a) Equivalent circuits of each modes. (b) Modifications of equivalent circuits.

Fig. 1 shows a schematic diagram of the proposed charger. The rectifier of the proposed charger is comprised of 6 diodes. The diodes D_1~D_4 are used for the resonant converter and D_5~D_6 are used for the FB converter. The outputs of the rectifiers are connected in series. These two converters are coupled with a single transformer, and the switches M_1~M_4 are commonly used for power control of the two converters.

B. Mode Analysis

Figs. 2 and 3 show key waveforms and operational mode diagrams of the proposed charger. The equivalent circuits of each mode are depicted in Fig. 4. Assuming that the magnetizing inductance of the transformer L_m is sufficiently large when compared with the resonant inductor L_r, the equivalent circuit can be redrawn as shown in Fig. 4(b) by exchanging the locations of L_r, the parallel network of L_m and n_1i_o.Where, n_1 is transformer turns-ratio of the FB converter and i_o is the output current. By modifying the equivalent circuits, the transformer primary current i_p can be divided into the three independent components of the magnetizing current i_m, the output current referred to the primary side n_1i_o, and the resonant current i_{Lr}. As a result, the two converter operations can be analyzed independently. Before analysis, it is assumed that the transformer has no leakage inductance and that all of the switching devices are ideal. In addition, the output voltage of the resonant converter v_{o_RC} has a constant value that is lower than the battery voltage V_{batt}, and the resonant capacitor voltage v_{cr} does not exceed V_{batt}. The detailed operational modes are explained as follows:

1) Mode 1 ($t_0 \leq t < t_1$): When M_1 is turned on at t_0, the primary current i_p flows through M_1, M_3, L_r, and the transformer primary; and the secondary current of the resonant converter i_{s_RC} is increased from zero in a resonant manner through C_r, D_1, D_3, C_{o2}, and the transformer secondary. Since i_{Lr} means the primary side current of the resonant converter, the relationship between i_{Lr} and i_{s_RC} is equal to $i_{Lr}=n_2 i_{s\_RC}$. From the equivalent circuit of mode 1, v_{cr}/n_2 and i_{Lr} can be expressed as follows:

$$\frac{v_{cr}(t)}{n_2}=\left(V_{in}-\frac{V_{o\_RC}}{n_2}\right)-\left(V_{in}+\frac{V_{cro}}{n_2}-\frac{V_{o\_RC}}{n_2}\right)\cos\omega_r t \quad (1)$$

$$i_{Lr}(t)=\frac{1}{Z_r}\left(V_{in}+\frac{V_{cro}}{n_2}-\frac{V_{o\_RC}}{n_2}\right)\sin\omega_r t \quad (2)$$

where, $\omega_r=1/[n_2\,(L_rC_r)^{0.5}]$ and $Z_r=(1/n_2)\,(L_r/C_r)^{0.5}$. In equations (1) and (2), n_2 is the transformer turns-ratio of the resonant converter, and v_{cr} is the resonant capacitor voltage. In addition, V_{cro} is the peak voltage of v_{cr}. Since the primary current i_p is the sum of i_m, n_1i_o, and i_{Lr}, it is written as:

$$i_p(t)=i_m(t)+n_1i_o(t)+i_{Lr}(t)=\frac{V_{in}}{L_m}(t)-\frac{V_{in}}{2L_m}DT_s+n_1i_o(t)+i_{Lr}(t) \quad (3)$$

where, L_m, T_s, and D refer to the magnetizing inductance, switching period, and duty-ratios of M_1 and M_4, respectively. During this mode, the transformer secondary voltage of the resonant converter v_{s_RC} is $V_{o\_RC}+v_{cr}$ and it appears at the transformer secondary voltage of the FB converter v_{s_FB} as (n_1/n_2) $(V_{o\_RC}+v_{cr})$. Thus, the output voltage of the FB rectifier v_x becomes $V_{o\_RC}+(V_{o\_RC}+v_{cr})(n_1/n_2)$ so that the voltage applied across the output inductor L_o can be written as follows:

$$v_L=V_{o\_RC}+\frac{n_1}{n_2}(v_{cr}+V_{o\_RC})-V_{batt} \quad (4)$$

2) Mode 2 ($t_1 \le t < t_2$): When M_1 is turned off and M_2 is turned on, the primary current i_p flows through M_3, the body diode of M_2, and the transformer primary; and the secondary current i_{s_RC} has same current path as that of mode 1 until i_{s_RC} is decreased to zero. From the equivalent circuit of mode 2, v_{cr}/n_2 and i_{Lr} can be expressed as follows:

$$\frac{v_{cr}(t)}{n_2}=-\frac{V_{o\_RC}}{n_2}-\left(-\frac{V_{cr}(t_1)}{n_2}-\frac{V_{o\_RC}}{n_2}\right)\cos\omega_r t+Z_r i_{Lr}(t_1)\sin\omega_r t \quad (5)$$

$$i_{Lr}(t)=\frac{1}{Z_r}\left(-\frac{V_{cr}(t_1)}{n_2}-\frac{V_{o\_RC}}{n_2}\right)\sin\omega_r t+i_{Lr}(t_1)\cos\omega_r t \quad (6)$$

$i_{Lr}(t_1)$ and $v_{cr}(t_1)/n_1$ in equations (5) and (6) are the initial conditions of mode 2 and they can be found from equations (1) and (2) as follows:

$$\frac{v_{cr}(t_1)}{n_2}=\frac{v_{cr}(DT_s)}{n_2}=\left(V_{in}-\frac{V_{o\_RC}}{n_2}\right)-\left(V_{in}+\frac{V_{cro}}{n_2}-\frac{V_{o\_RC}}{n_2}\right)\cos\omega_r DT_s \quad (7)$$

$$i_{Lr}(t_1)=i_{Lr}(DT_s)=\frac{1}{Z_r}\left(V_{in}+\frac{V_{cro}}{n_2}-\frac{V_{o\_RC}}{n_2}\right)\sin\omega_r DT_s \quad (8)$$

In addition, since the transformer primary is shorted by the M_2 and M_3 switches, the magnetizing current i_m is kept constant.

Therefore, i_p becomes:

$$i_p(t-t_1)=\frac{V_{in}}{2L_m}DT_s+n_1i_o(t)+i_{Lr}(t-t_1) \quad (9)$$

This mode continues until i_{Lr} is decreased to zero and its duration can be derived as the following equation with equations (6)-(8).

$$T_{M2}=\frac{1}{\omega_r}\tan^{-1}\left(-\frac{b}{a}\right) \quad (10)$$

Where:

$$a\equiv -V_{in}+\left(V_{in}+\frac{V_{cro}}{n_2}-\frac{V_{o\_RC}}{n_2}\right)\cos\omega_r DT_s$$

$$b\equiv\left(V_{in}+\frac{V_{cro}}{n_2}-\frac{V_{o\_RC}}{n_2}\right)\sin\omega_r DT_s$$

Referring to the key waveforms and operational mode diagram of mode 2, the conduction path of the rectifiers in the resonant converter is kept the same as that of mode 1. Thus, v_x is maintained as $V_{o\_RC}+(V_{o\_RC}+v_{cr})(n_1/n_2)$ and the operation of the FB converter is the same as that of mode 1.

3) Mode 3 ($t_2 \le t < t_3$): After i_{s_RC} is decreased to zero, the diodes D_1 and D_3 are turned off and only the magnetizing current i_m and output current referred to the primary side n_1i_o circulate together through M_3 and the body diode of M_2. In addition, the resonant capacitor voltage v_{cr} is maintained as $v_{cr}(t_2)$. Since $v_{cr}(t_2)$ is equal to V_{cro}, it can be derived as the following equation with equations (5) and (10).

$$v_{cr}(t_2)=V_{cro}=\frac{n_2V_{in}(n_2V_{in}-V_{o\_RC})(1-\cos\omega_r DT_s)}{2V_{o\_RC}-n_2V_{in}(1-\cos\omega_r DT_s)} \quad (11)$$

To prevent abnormal turn-on of the rectifying diodes of the resonant converter during mode 3, the maximum value of V_{cro} should not exceed V_{o_RC} of the proposed converter. Thus, the resonant parameters should be designed to meet this condition and this is imposed as one of the design guidelines. When M_3 is turned off and M_4 is turned on, the next half cycle begins and its operation is similar to the previous half cycle.

C. Voltage Gain of the Proposed Converter

Referring to Fig. 2, the voltage waveform applied across the output inductor can be depicted as Fig. 6. In order for the inductor current to stay in the stead-state, the following condition should be satisfied.

$$\frac{2}{T_s}\left[\int_0^{DT_s+T_{M2}} V_{o2}+\frac{n_1}{n_2}(v_{cr}+V_{o\_RC})-V_{batt}dt+(V_{o\_RC}-V_{batt})(T_s-DT_s-t_x)\right]=0 \quad (12)$$

Since the average value of v_{cr} during DT_s+T_{M2} is equals to zero in the steady-state, the relationship between V_{batt} and V_{o_RC} can be derived from equation (12) as follows:

$$V_{batt}=\frac{n_1}{n_2}V_{o\_RC}\left(D+\frac{T_{M2}}{T_s}\right)+V_{o\_RC} \quad (13)$$

To derive the relationship between V_{co2} and I_o, information on the input power that the resonant converter is responsible for is required. The input current i_{in} is the sum of i_{M1} and i_{M4}, and i_{M4} has the same waveform as i_{M1} except for a phase delay of 180^o. Thus, it is sufficient to consider the input current during half a cycle. Referring to Fig. 2, i_{M1} is equal to ip during mode 1, and i_p is expressed as equation (3). Accordingly, it can be seen that the average input power of the resonant converter $P_{in,R}$ can be calculated by averaging the product of v_{in} and i_{Lr} over half of the switching cycle. From equations (2) and (11), it can be derived that:

$$P_{in.R}=\frac{2}{T_s}\int_0^{T_s/2} v_{in}(t)i_{Lr}(t)dt=\frac{2V_{in}n_2^2C_r}{T_s}\frac{2\frac{V_{o\_RC}}{n_2}\left(V_{in}-\frac{V_{o\_RC}}{n_2}\right)\times Q}{2\frac{V_{o\_RC}}{n_2}-V_{in}Q} \quad (14)$$

where, Q=1−cos$\omega_r DT_s$. The output power of the resonant converter $P_{o,R}$ can be expressed as:

$$P_{o2}=V_{o\_RC}I_o \quad (15)$$

By equating equation (14) with equation (15), V_{o_RC} can be derived as:

$$\frac{V_{o\_RC}}{n_2}=\frac{4V_{in}^2n_2^2C_rQ+V_{in}I_oT_sQ}{2I_oT_s+4V_{in}n_2^2C_rQ} \quad (16)$$

Therefore, the battery voltage can be written as follows:

$$V_{batt}=\left[n_1\left(D+\frac{t_x}{T_s}\right)+n_2\right]\left(\frac{4V_{in}^2n_2^2C_rQ+V_{in}I_oT_sQ}{2I_oT_s+4V_{in}n_2^2C_rQ}\right) \quad (17)$$

D. ZVS Switching Condition

Fig. 5 shows the expanded switching waveforms to illustrate the ZVS operation and equivalent circuits during T_{dead} of the dead-time between the gate signals of top and bottom switches. Where, C_{ds} is the drain-source capacitance of the primary switches. Referring to these figures, the ZVS conditions of M_2 and M_3 are easily satisfied because the peak current of i_p is used for ZVS. However, the ZVS of M_1 and M_4 is only aided by the magnetizing current and output current referred to the primary side [11]. Assuming that the dead-time is short enough for the magnetizing current during dead-time to be constant and that the output current ripple is negligibly small, the magnitude of i_p during the dead-time between M_1 and M_4 can be found as follows:

$$i_p=I_{m,pk}+n_1i_o\approx\frac{V_{in}}{2L_m}DT_s+n_1I_o \quad (18)$$

This current changes the potentials of the output capacitances of the top and bottom switches from zero to the input voltage. Referring to the equivalent circuit in Fig. 5, the potential changing time ΔT can be derived as follows:

$$\Delta T=\frac{2C_{ds}V_{in}}{\frac{V_{in}}{2L_m}DT_s+n_1I_o} \quad (19)$$

To achieve the ZVS of M_1 and M_4, ΔT should be shorter than T_{dead}. From this condition, for L_m to meet ZVS can be found as follows:

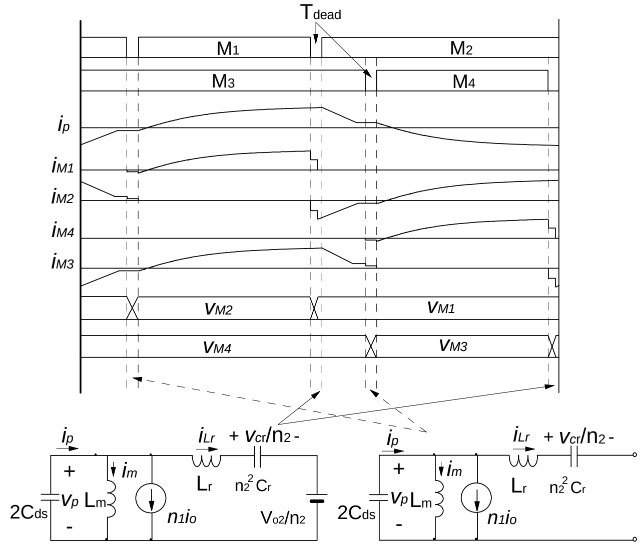

Fig. 5. Expanded switching waveforms and equivalent circuits during dead-times.

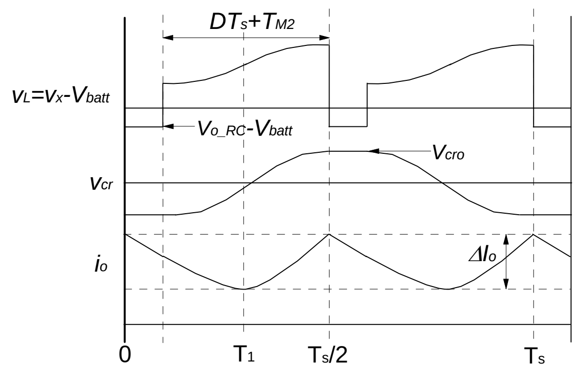

Fig. 6. Waveforms of the voltage applied across output inductor v_L, resonant capacitor voltage v_{cr}, and inductor current ripple Δi_o.

$$L_m\le\frac{V_{in}DT_s}{2\left(\frac{2C_{ds}V_{in}}{T_{dead}}-n_1I_o\right)} \quad (20)$$

The worst case for selecting L_m happens at D_{min} and $I_{o,min}$, that is, the minimum battery voltage and the minimum charging current. Since values of D_{min} and $I_{o,min}$ that are too small increase the circulating current and the turn-off switching loss of the upper switches. Proper values of D_{min} and $I_{o,min}$ should be selected considering the operational characteristics of the charger.

E. Voltage Stresses of the FB Output Diodes

During the powering durations from mode 1 to mode 2, the transformer secondary voltage of the resonant converter stage v_{s_RC} is v_{cr}+ V_{o_RC}. As a result, the transformer secondary voltage of the FB stage v_{s_FB} becomes $(n_1/n_2)(v_{cr}+V_{o\_RC})$. The anode-to-cathode voltage of the diode in the FB stage is twice v_{s_FB}. Because mode 3 is the freewheeling duration, the maximum voltage stress occurs at the end of mode 2, and it can be written as follows:

$$V_{D5,6\_\max} = 2\frac{n_1}{n_2}(v_{cr}(t_2) + V_{o\_RC}) = 2\frac{n_1}{n_2}(V_{cro} + V_{o\_RC}) \quad (21)$$

From equation (21), it can be known that if n_1 is a lot smaller than n_2, the voltage stress of D_5 and D_6 can be reduced to the level where Schottky diodes with a low on-drop voltage are available. In addition, the leakage inductance is used for the resonant parameter so that the voltage spikes caused by the diode junction capacitance and leakage inductance do not exist.

F. Output Inductor Ripple

Fig. 6 shows waveforms of the voltage applied across the output inductor v_L, the resonant capacitor voltage v_{cr}, and the inductor current ripple Δi_o. With equation (4), Δi_o can be written as:

$$\Delta i_o = \int_{T_1}^{T_s/2} \frac{v_L}{L_o} dt = \frac{1}{L_o}\int_{T_1}^{T_s/2}\left(V_{o\_RC} + \frac{n_1}{n_2}(v_{cr} + V_{o\_RC}) - V_{batt}\right)dt \quad (22)$$

To derive the design equation of the output inductor, the following assumptions are made:

1) The duration of mode 3 is small enough to be zero at the maximum battery voltage and maximum load.
2) The waveforms of v_{cr} during mode 1 and mode 2 are near to a sinusoidal waveform.

From these two assumptions, DT_s+T_{M2}, T_1, and v_{cr} can be approximated as $T_s/2$, $T_s/4$, and $-V_{cro}\cos(2\pi t/T_s)$, respectively. Therefore, equation (23) can be rewritten as:

$$\Delta i_o \approx \frac{1}{L_o}\left[\frac{T_s}{4}\left(V_{o2} + \frac{n_1}{n_2}V_{o\_RC} - V_{batt}\right) - \frac{n_1}{n_2}\int_{T_s/4}^{T_s/2} V_{cro}\cos(2\pi t/T_s)dt\right] \quad (23)$$

In addition, the inductor current ripple Δi_o at the maximum load condition can be derived as follows:

$$\Delta i_o = \frac{1}{L_o}\left[\frac{T_s}{4}\left(V_{o\_RC} + \frac{n_1}{n_2}V_{o\_RC} - V_{batt}\right) + \frac{n_1}{n_2}\frac{T_s}{2\pi}V_{cro}\right] \quad (24)$$

III. Design Procedure

As mentioned in the mode analysis in Section II, the resonant parameters should be designed to meet the condition that V_{cro} does not exceed V_{batt}. In addition, the duration from mode 1 to mode 2, DT_s+T_{M2} should be shorter than $T_s/2$ to minimize the turn-off switching losses of the bottom switches and the output diodes. Therefore, some design procedures to meet the design conditions are given below.

Step 1: Select D_{max}, n_2, and V_{o_RC}.

Referring to equation (11), V_{cro} should not have a negative value so that n_2V_{in} should be larger than the maximum V_{o_RC}. Based on this condition, the range of n_2 that guarantees normal operation can be written as:

$$n_2 \geq \frac{V_{o\_RC,\max}}{V_{in}} \quad (25)$$

From equation (16), it can be known that the minimum n_2 happens when the duty-ratio D is equal to 0.5 and the switching frequency f_s is equal to the resonant frequency f_r. These conditions mean that the converter has complete resonant operation. However, the operational duty-ratio is used below 0.5 to guarantee the duration of mode 1, and f_s is always higher than f_r for the PWM control. Therefore, n_2 should be selected with a value that is sufficiently larger than the minimum value resulting from equation (25). Finally, the maximum operational duty-ratio D_{max} is chosen considering the duration of mode 2.

Step 2: Find the resonant frequency ω_r.

Using equations (10) and (11) and the selected values in step 1, V_{cro} and T_{M2} can be plotted according to the resonant frequency ω_r at $V_{batt,max}$ and V_{in}. From this plot, an appropriate resonant frequency can be chosen to meet the conditions of $V_{cro} < V_{batt,max}$ and $DT_s+ T_{M2} <T_s/2$.

Step 3: Find the resonant tank parameters.

From the results of step 2 and equation (16), a resonant capacitor C_r can be selected to meet the condition that the value of V_{o_RC} calculated at D_{max} is equal to or slightly larger than the selected $V_{o\_RC,max}$. After that, the resonant inductor L_r is calculated with the selected C_r and n_2.

Step 4: Find n_1.

With T_{M2} found in step 2, and $V_{o\_RC,max}$ recalculated in step 3, the minimum n_1 can be obtained using equation (13).

Step 5: Check whether the design meets the conditions of V_{cro} $<V_{batt}$ and $DT_s+T_{M2}<T_s/2$ under all of the battery voltage ranges.

It is sufficient that this step be performed at the maximum charging powers according to the battery voltages because V_{cro} and DT_s+T_{M2} are increased as the load becomes heavy.

IV. Design and Experimental Results

A 6.6kW prototype charger has been designed (V_{in}=400V, V_{batt}=250V~420V/$I_{o,max}$=20A) and its switching frequency is 50kHz.

Step 1: As mentioned in the design procedure, $V_{o\_RC,max}$ should be smaller than the maximum battery voltage to guarantee proper operation. Therefore, $V_{o\_RC,max}$ was selected as 394V. From this selected value, the minimum turns-ratio of n_2 becomes 0.985 from equation (25). To secure the duration of mode 2, 0.35 was selected for D_{max}, and 1.2 was used for n_2 considering the maximum operational duty-ratio.

Step 2: Fig. 7 shows the plots of DT_s+T_{M2} and V_{cro} according to resonant frequency variations with the selected values of step 1 and equations (10) and (11) at V_{in}=400V and $V_{o\_RC,max}$=394V. From this figure, DT_s+T_{M2} and V_{cro} has been selected as 8.97μs and 163V at ω_r=235krad/sec in this design.

Step 3: From the results of step 2 and equation (16), the voltage gain of the resonant converter can be plotted as shown in Fig. 8 according to variations of C_r. In order for the

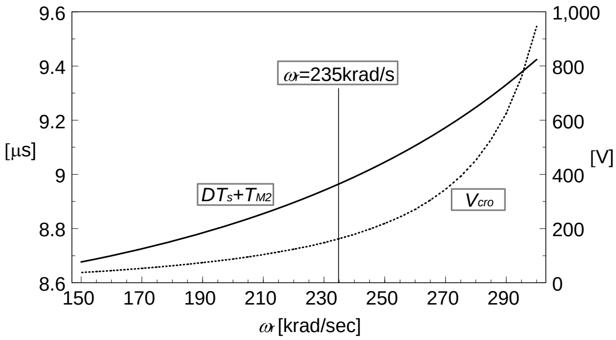

Fig. 7. Plot of DT_s+T_{M2} and V_{cro} according to resonant frequency variations with the selected values of step 1 at V_{in}=400V and $V_{o\_RC,max}$=394V.

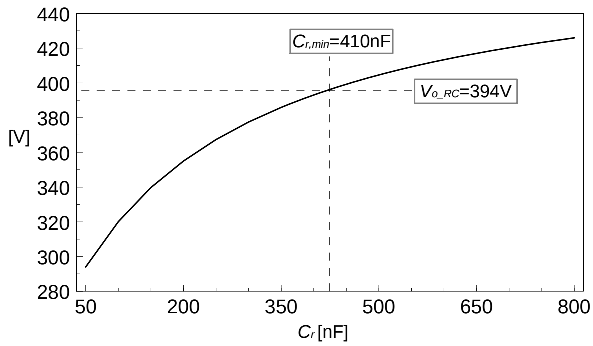

Fig. 8. Output voltage of resonant converter stage according to C_r variations at maximum load conditions.

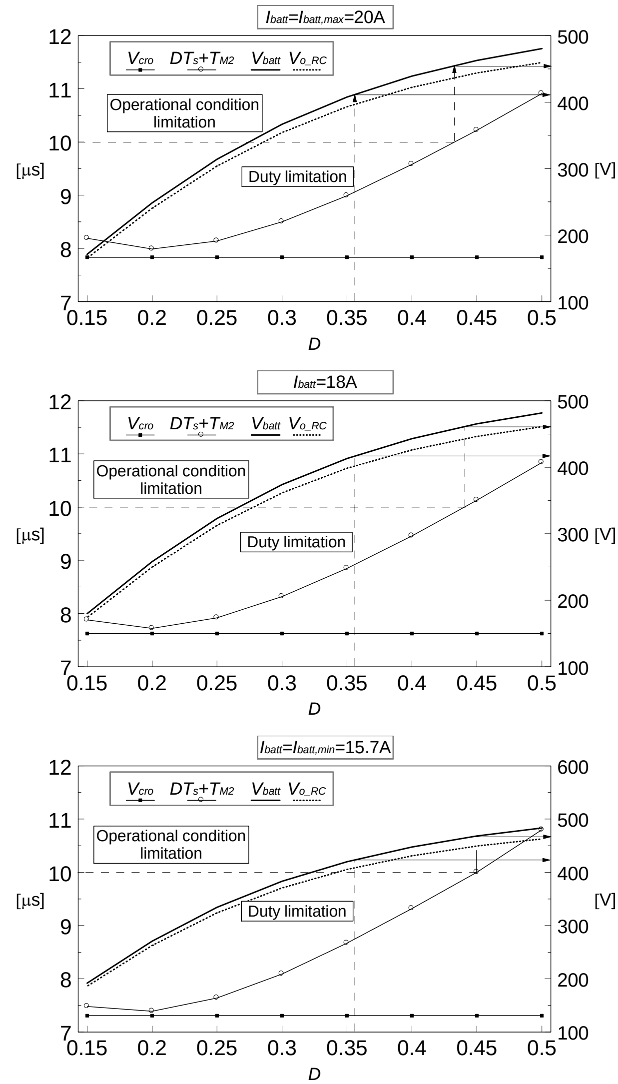

Fig. 9. Plots of V_{cro}, V_{batt}, and DT_s+T_{M2} according to duty-ratio variations and charging profile

prototype converter to meet the selected value of $V_{o\_RC,max}$, the minimum voltage gain of the converter must be 0.985. The minimum value of C_r to meet this gain is 410nF. However, too large a C_r increases the switch current stresses as shown in equation (2). Thus, C_r=500nF has been selected, and 25.1µH of L_r was calculated as a result.

Step 4: Since C_r is selected so that the gain of the resonant converter is larger than 0.985, $V_{o\_RC,max}$ is recalculated and it is 405V. Using this recalculated $V_{o\_RC,max}$, the minimum value of n_1 can be found using equation (13). The calculated value is 0.0991 and 0.1 has been used in this design.

Step 5: Fig. 9 shows the plot of V_{cro}, V_{batt}, V_{o_RC}, and DT_s+T_{M2} according to the duty-ratio and charge current variations using equations (10), (11), (16), and (17). This figure shows that the maximum chargeable voltage at $I_{batt,max}$=20A is 407.7V under the duty-ratio limitation and that it is 458V under the operational condition limitation. In addition, the maximum chargeable voltage at $I_{batt,max}$=15.7A is 420V under the duty-ratio limitation and it is 468V under the operational condition limitation. According to this figure, the design can meet the normal operational conditions of $V_{cro}< V_{o\_RC}$ and $DT_s+T_{M2}<T_s/2$ under all of the battery voltage ranges. From Fig. 9, it can be known that the difference between V_{o_RC} and V_{cro} becomes larger as V_{batt} increases, while V_{cro} is kept nearly constant. Thus, these converter characteristics and equation (24) show that the maximum current ripple happens at the maximum battery voltage. Referring to Fig. 9, V_{o_RC} and V_{cro} at V_{batt}=420V are 405.4V and 130.8V, respectively. Therefore, L_o can be calculated as 65µH when the output current ripple is selected as 10% of a maximum current of 20A. This is a very low inductor value compared with conventional FB chargers because a FB charger having the same specifications as the proposed charger requires an output inductor that is around 2mH. In addition, the low current ripple of the proposed charger provides another merit since a bulky current filter is not required. As mentioned in section III, the worst case for selecting L_m happens at D_{min} and $I_{o,min}$ and they are 0.2 and 20A from Fig. 9. Using this information and the selected devices, L_m can be calculated as about 286µH at T_{dead}=300ns. In this design, 256µH has been used. Fig. 10 shows the implemented prototype, and Table I presents a key components list of the prototype charger. It shows that A_p of the transformer in the proposed charger is 61.5cm^4 at a 6.6kW output, while those in references [12] and [13] are

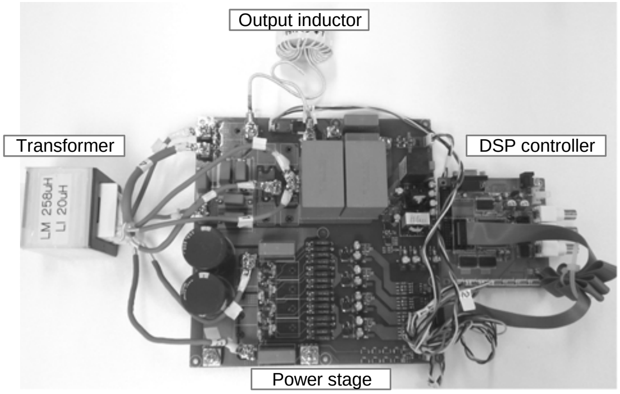

Fig. 10. Implemented prototype.

TABLE I
KEY COMPONENT LIST

Component	Implementation
M_1~M_4	IPW65R041CFD×2
D_1~D_2	DSSK 60-02A
D_4~D_6	FFH50US60S
Transformer	$1{:}n_1{:}n_2$=1:0.1:1.2 (EE6565 × 2 stack) L_{lkg}=25μH, L_m=256μH, A_p=61.5cm^4
L_o	65μH(CH467060 High flux core)
C_r	500nF (Film capacitor)
C_o	200μF

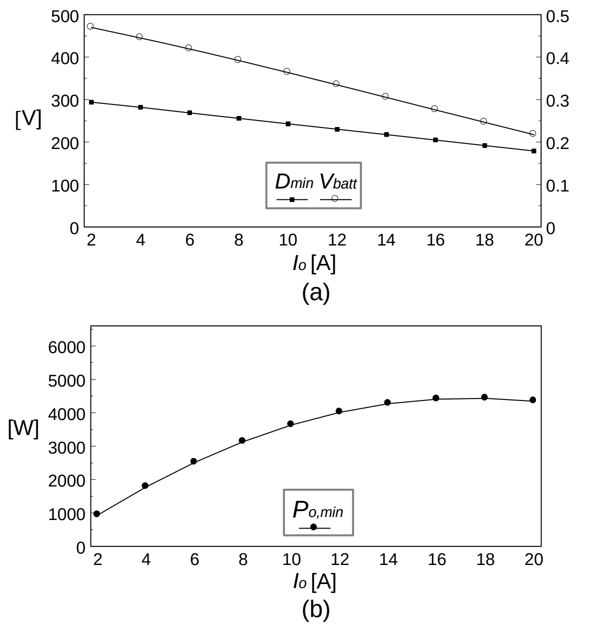

Fig. 11. Battery voltages calculated at (a) minimum duty-ratios to meet ZVS of M_1 (or M_4) and (b) minimum load conditions for ZVS of M_1 (or M_4).

89.32cm^4 at a 3.5kW output, where A_p means the product of the window area and the cross-sectional area of the transformer core. Fig. 11(a) shows the battery voltages at the minimum duty-ratios to meet the ZVS calculated with equations (17) and (20). From this figure, it can be seen that the minimum load conditions for the ZVS of M_1 (or M_4) can

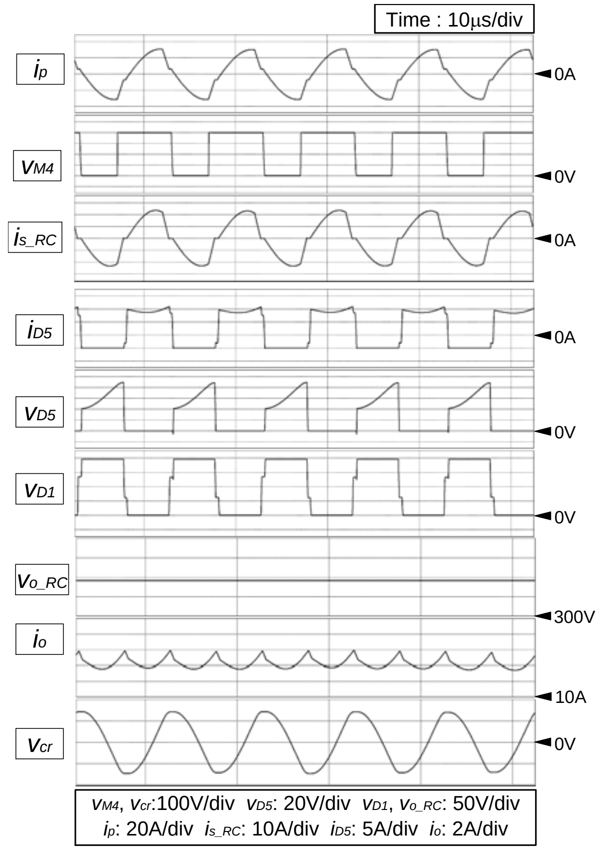

Fig. 12. Simulated switching waveforms measured at V_{batt}=420V /P_o=6.6kW.

be depicted according to battery current, as shown in Fig. 11(b). The ZV-ZCS of M_2 (or M_3) is met under the overall load range due to its switching characteristics as explained in the mode analysis. Figs. 12 and 13 show switching waveforms simulated and measured at V_{batt}=420V/P_o=6.6kW. The switching waveforms show good agreement with the theoretical analysis. In addition, the output current ripples are below 2A under the entire battery voltage range with a small output inductor. The ringing voltage of V_{D1} is caused by resonance between the diode junction capacitance and the resonant inductor reflected to the secondary side. In addition, the parasitic inductance of the interconnection causes the very high frequency voltage spike of V_{D5} with the diode junction capacitance. Fig. 14 shows the measured current and voltage waveforms of M_1 and M_2. Form this figure, the ZVS of the upper switch and the ZV-ZCS of the lower switch are well accomplished. Fig. 15 shows the measured efficiency according to the battery voltages. The efficiency has been measured with a YOKOGAWA WT500 power analyzer. It shows that a 97.2% efficiency has been recorded at 360V/6.6kW and that a maximum efficiency of 97.4% has been measured at 413V/6.6kW. Although the rectifier is comprised of 6 diodes and all of the diodes are used for carrying battery charging current, serious efficiency degradation does not occur because the maximum increase of

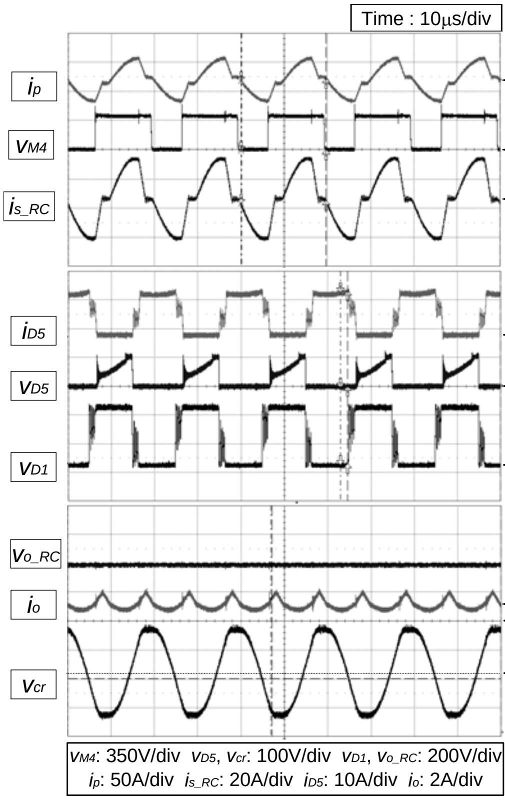

Fig. 13. Switching waveforms measured at V_{batt}=420V /P_o=6.6kW.

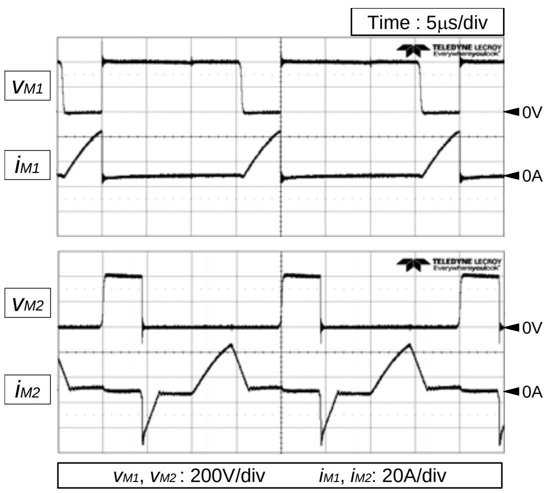

Fig. 14. Measured current and voltage waveforms of M_1 and M_2.

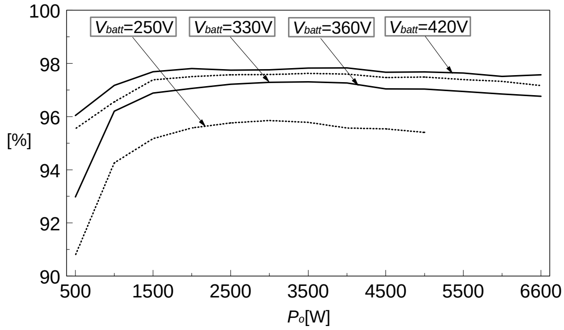

Fig. 15. Measured efficiency according to battery voltages.

the rectifier conduction loss contributed by the Schottky diodes of the FB stage is approximately 14W when the battery charging current is at its maximum.

V. Conclusions

A hybrid PWM DC/DC converter comprised of a FB converter and a resonant converter has been proposed for OBCs. The proposed converter has the mixed operational characteristics of the two converters and all of them use PWM, which simplifies the transformer structure by coupling the two secondary sides. The switching characteristics are similar to those of a PWM resonant converter so that the ZV-ZCS operation of at the bottom switches and the ZVS operation of the top switches can be accomplished by proper design of the resonance. In addition, the proposed structure provides merits such as no dissipative snubber circuitry and no output filter. Some analyses to explain the operation of the charger and select its design parameters has been performed. Based on these analyses, design equations have been derived. To verify the performance, a 6.6KW prototype charger has been implemented with the design guidelines. Experimental results show that a maximum efficiency of 97.4% has been obtained at 413V/6.6kW. Therefore, it may be suitable for the DC/DC stage in single-phase PHEV/EV chargers requiring high efficiency.

Acknowledgment

This work was supported by the National Research Foundation of Korea(NRF) grant funded by the Korea government(MSIP)(NRF-2015R1A2A2A01004102) and the Korea Institute of Energy Technology Evaluation and Planning(KETEP) grant funded by the Korea government(MOTIE)(No. 20162020107590)

References

[1] A. Y. Saber and G. K. Venayagamoorthy, “Plug-in vehicles and renewable energy sources for cost and emission reductions,” *IEEE Trans. Ind. Electron.*, Vol. 58, No. 4, pp. 1229-1238, Apr. 2011.

[2] M. Rosekeit and R.W. De Doncker, “Smoothing power ripple in single phase chargers at minimized dc-link capacitance,” in *Proc.IEEE ICPE ECCE*, 2011, pp. 2699-2703.

[3] A. Khaligh and S. Dusmez, “Comprehensive topological analysis of conductive and inductive charging solutions for plug-in electric vehicles,” *IEEE Trans. Veh. Technol.*, Vol. 61, No. 8, pp.3475-3489, Oct.2012.

[4] F. Musavi, M. Craciun, D. S. Gautam, W. Eberle, and W. G. Dunford “An LLC resonant DC-DC- converter for wide output voltage range battery charging applications,” *IEEE Trans. Power Electron.*, Vol. 28, No. 12, pp. 5437-5445, Dec. 2013.

[5] Haoyu Wang, Serkan Dusmez, and Alireza Khaligh. “A

novel approach to design EV battery chargers using SEPIC PFC stage and optimal operating point tracking technique for LLC converter," in *Proc. IEEE Appl. Power Electron. Conf. Expo*., pp. 1683-1689, 2014.
[6] B. Ren Lin and W. J Lin, "Half-bridge zero voltage switching converter with three resonant tanks," *Journal of Power Electronics*, Vol. 14, no 5, pp. 882-889, Sep. 2014.
[7] S. G. Kim and F. S. Kang, "Multifunctional onboard battery charger for plug-in electric vehicles," *IEEE Trans. Ind. Electron*., Vol.62, No. 6, pp.3460-3472, Jun.2015.
[8] M. Grenier, M. G. Hosseini Aghdam, and T. Thiringer, "Design of on-board charger for plug-in hybrid electric vehicle," in *Proc.IEEE PEMD*, 2010, pp. 1-6.
[9] H. J. Chae, H. T. Moon, and J. Y. Lee, "On-board battery charger for PHEV without high voltage electrolytic capacitor," *Electron. Lett*., Vol.46, No. 25, pp. 1691-1692, Dec. 2010.
[10] P. Reid, C. Mittelstadt, and T. Faber, "Electric vehicle conductive charge couplers," in *Proc. IEE 60th Holm Conf. Electr. Contacts*, 2014, pp. 1-7.
[11] B. K. Lee, J. P. Kim, S. G. Kim, and J. Y. Lee, "A PWM SRT DC/DC Converter for 6.6-kW EV Onboard Charger," *IEEE Trans. Ind. Electron.*, Vol. 63, No. 2, pp. 894-902, Feb. 2016
[12] W. Yu, J. D. Lai, W. H. Lai, and H. Wan, "Hybrid resonant and PWM converter with high efficiency and full soft-switching range," *IEEE Trans. Ind. Electron*., Vol. 27, No. 2, pp. 4925-4932, Dec. 2012.
[13] C. Liu, B. Gu, J. S. Lai, M. Wang, Y. Ji, G. Cai, Z. Zhao, C. L. Chen, C. Zheng, and P. Sun, "High-efficiency hybrid full-bridge–half-bridge converter with shared zvs lagging leg and dual outputs in series," *IEEE Trans. Power Electron.*, Vol. 28, No. 2, pp. 849-861, Feb. 2013.

Najam ul Hassan was born in Karachi, Pakistan, in 1985. He received his B.S. degree in Telecommunication Engineering from the National University of Computer and Emerging Sciences, Peshawar, Pakistan, in 2009. Since 2015, he has been working towards his M.S. degree in Electrical Engineering at Myongji University, Seoul, Korea. His current research interests include power electronics applications with dc/dc bi-directional converters, ac/dc PFC converters, and battery chargers.

Yoon-Jae Kim was born in Busan, Korea, in 1985. He received his B.S. degree in Electrical Engineering from Gwangwoon University, Seoul, Korea, in 2012. From 2012 to 2015, he worked as a Researcher in the Motor Driver Development Group, Justek Inc., Pyeongtaek, Korea, where he was involved in circuit and product development. He is currently working towards his M.S. at Myongji University, Seoul, Korea. His current research interests include power electronics applications with dc/dc bi-directional converters, ac/dc PFC converters, and battery chargers.

Byung-Moon Han received his B.S. degree in Electrical Engineering from Seoul National University, Seoul, Korea, in 1976; and his M.S. and Ph.D. degrees from Arizona State University, Phoenix, AZ, USA, in 1988 and 1992, respectively. He was with the Westinghouse Electric Corporation as a Senior Research Engineer in the Science & Technology Center, Pittsburg, PA, USA. He is presently working as a Professor in the Department of Electrical Engineering, Myongji University, Seoul, Korea. His current research interests include power electronics applications for FACTS devices, custom power, distributed generation, and microgrids.

Jun-Young Lee received his B.S. degree in Electrical Engineering from Korea University, Seoul, Korea, in 1993; and his M.S. and Ph.D. degrees in Electrical Engineering from the Korea Advanced Institute of Science and Technology (KAIST), Taejon, Korea, in 1996 and 2001, respectively. From 2001 to 2005, he worked as a Manager in the Plasma Display Panel Development Group, Samsung SDI, Korea, where he was involved in circuit and product development. From 2005 to 2008, he worked as a faculty member in the School of Electronics and Computer Engineering, Dankook University, Yongin, Korea. In 2008, he joined the School of Electrical Engineering, Myongji University, Seoul, Korea, as a Professor. His current research interests include power electronics, converter topology design, soft switching techniques, plasma power, soft-switching inverters, and battery charging systems.